Metal–Radical Complexes

DOI: 10.1002/anie.200701600

Generation of a Ru^{II}–Semiquinone–Anilino-Radical Complex through the Deprotonation of a Ru^{III}–Semiquinone–Anilido Complex**

*Yuji Miyazato, Tohru Wada, James T. Muckerman, Etsuko Fujita, and Koji Tanaka**

Aminyl radicals are thermodynamically unstable and are able to oxidize organic substrates through H-atom abstraction.[1] Metal complexes that contain aminyl radicals may therefore have the potential to function as new oxidation catalysts in organic synthesis. The actual electronic state of an aminyl-radical–metal complex should lie somewhere between two limiting resonance structures, the amido state ($M^{(n+1)+}$–$^{-}NR_2$) and the aminyl radical (M^{n+}–$^{\bullet}NR_2$; Scheme 1 a),[2–4] and would usually be shifted toward the former. Recently, metal complexes with aminyl radicals were isolated by chemical and electrochemical oxidation of the corresponding metal–amido complexes.[2] The Ru^{II}–semiquinone–oxyl radical complex [Ru^{II}(terpy)(tBu$_2$sq)(O$^{\bullet-}$)] (terpy = 2,2′:6′,2′′-terpyridine, tBu$_2$sq^{-} = 3,5-di-*tert*-butylsemiquinonate) was isolated through the deprotonation of [Ru^{III}(terpy)(tBu$_2$sq)(OH)]$^{+}$ under basic conditions without the use of an oxidant.[5] Furthermore, the deprotonated species derived from [Ru^{III}(terpy)(tBu$_2$sq)(NH$_3$)]$^{2+}$ and [Ru^{III}(NH$_2$CH$_2$CH$_2$-bpa)(tBu$_2$sq)]$^{2+}$ (NH$_2$CH$_2$CH$_2$-bpa = bis(2-pyridylmethyl)-2-aminoethylamine) were shown to oxidize alcohols to aldehydes or ketones with the generation of [Ru^{II}(terpy)(tBu$_2$sq)(NH$_3$)]$^{+}$ and [Ru^{II}(NH$_2$-bpa)(tBu$_2$sq)]$^{+}$, respectively.[6,7] The most plausible active species for the oxidation of alcohols is a Ru^{II}–semiquinone–aminyl radical, which is a limiting resonance structure of an Ru^{III}–semiquinone–amido complex (Scheme 1 b). The Ru^{II}–semiquinone–aminyl radical intermediate was too labile to identify its existence in oxidation reactions. However, analogous Ru^{III}–semiquinone–anilino-radical complexes, which would be formed from the corresponding Ru^{III}–semiquinone–aniline complexes, may be stabilized by the π conjugated system of the aniline group.

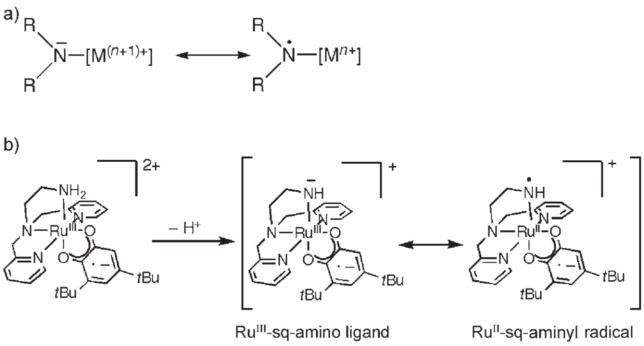

Scheme 1. a) Resonance between metal-coordinated amido and aminyl-radical species; b) a proposed mechanism for the formation of a Ru^{II}–semiquinone–aminyl-radical intermediate.

Herein we describe the preparation of the Ru^{II}–semiquinone–anilino radical [Ru^{II}($^{\bullet}$NPh-bpa)(tBu$_2$sq)]·2 H$_2$O (**2**) and the related species derived from **2** by one-electron reduction, that is, the Ru^{II}–catechol–anilino radical [Ru^{II}($^{\bullet}$NPh-bpa)(tBu$_2$cat)]$^{-}$ (**3**). Both complexes contain the 2-(bis(2-pyridylmethyl)aminomethyl)anilido ligand (NPh-bpa^{2-}).[8] The anilino-radical character of **2** and **3** was proved by EPR spectroscopy, resonance Raman spectroscopy, and DFT calculations.

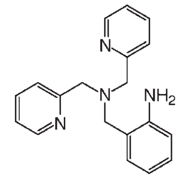

NH$_2$Ph–bpa

The Ru^{III}–semiquinone–anilido complex [Ru^{III}(NHPh-bpa)(tBu$_2$sq)]$^{+}$ (**1**) was obtained with the counterion ClO$_4^{-}$ and one equivalent of water of crystallization after treatment of [{Ru^{II}(NH$_2$Ph-bpa)}$_2$(μ-Cl)$_2$](PF$_6$)$_2$ with AgBF$_4$, 3,5-di-*tert*-butylcatechol, and tBuOLi in a mole ratio of 1:2:2:4 in acetone. An N–H vibration was observed at 3266 cm^{-1} by IR spectroscopy. The UV/Vis/NIR spectrum of **1** in CH$_2$Cl$_2$ showed four sharp charge-transfer (CT) bands at 370 (4980), 558 (5070), 872 nm (9450 M^{-1}cm^{-1}), and 1172 nm (4470 M^{-1}cm^{-1}). X-ray photoelectron spectroscopy of **1** indicated a binding energy of 282.1 eV for Ru^{III} at the 3$d_{5/2}$ level.[9] The effective magnetic moment of **1** at 300 K was found to be 0.86 μ$_B$ which is much smaller than the spin-only value (2.45 μ$_B$) expected for $S_1 = S_2 = \frac{1}{2}$ for the {Ru^{III}–sq} framework. Furthermore, **1** is EPR inactive at 5 K, which indicates that a strong antiferromagnetic interaction operates within the {Ru^{III}–sq} framework of **1** (see the Supporting Information).

The anilido moiety of **1** undergoes deprotonation with tBuOK in dimethoxyethane (DME) to afford [Ru^{II}($^{\bullet}$NPh-bpa)(tBu$_2$sq)]·2 H$_2$O (**2**) rather than [Ru^{III}(NPh-bpa)-

---

[*] Dr. Y. Miyazato, Dr. T. Wada, Prof. K. Tanaka
Institute for Molecular Science
5-1 Higashiyama, Myodaiji, Okazaki, Aichi, 444-8787 (Japan)
Fax: (+81) 564-59-5582
E-mail: ktanaka@ims.ac.jp
Dr. J. T. Muckerman, Dr. E. Fujita
Brookhaven National Laboratory
Upton, NY 11973-5000 (USA)

[**] We thank Prof. T. Yokoyama and Dr. T. Nakagawa at the Institute for Molecular Science for measuring the X-ray photoelectron spectra (XPS) and the Research Center for Molecular-Scale Nanoscience at the Institute for Molecular Science for measurements with the SQUID magnetometer. This research was supported financially by a Grant-in-Aid for Scientific Research on Priority Areas (No. 18033057). Research carried out at the Brookhaven National Laboratory was funded by the Division of Chemical Sciences, Geosciences, & Biosciences, Office of Basic Energy Sciences of the U.S. Department of Energy under the contract DE-AC02-98CH10886.

Supporting information for this article is available on the WWW under http://www.angewandte.org or from the author.

(tBu$_2$sq)]·2H$_2$O (Scheme 2). The deprotonation was confirmed by the disappearance of the N–H vibration band. The UV/Vis/NIR spectrum of **2** in CH$_2$Cl$_2$ at room temperature exhibited intense CT bands at 366 (6620), 638 (5210), and 906 nm (5060 $\text{M}^{-1}\text{cm}^{-1}$). The noncoordinated anilino radical undergoes a π–π* transition at 400 nm. Characteristic ν_{8a} (C_{ortho}–C_{meta} stretching in the phenyl ring) and ν_{7a} (C–N stretching) vibrational modes were observed at 1560 and 1505 cm^{-1}, respectively, in the resonance Raman spectrum obtained by excitation of the π–π* transition.[10] In the electronic absorption spectrum of **2**, a discernible increase in the absorbance relative to that of **1** in the region of 400 to 500 nm presumably results from the generation of the anilino radical species (see the Supporting Information). The resonance Raman spectrum obtained by the excitation at 514.5 nm of **2** in CH$_2$Cl$_2$ at room temperature (Figure 1) contained bands at 1611 and 1552 cm^{-1} which were not detected for **1**. Thus, we assigned these bands to the ν_{8a} and ν_{7a} vibrational modes of the anilino radical moiety, respectively. The EPR spectrum of **2** in CH$_2$Cl$_2$ at 5 K showed two significant transitions at approximately $g = 2$ and at $g = 4.2$ for the spin-triplet system, whereas **1** was EPR inactive at 5 K as a result of the strong antiferromagnetic interaction between Ru^{III} and the semiquinonate ligand. Simulation of the EPR spectrum resulted in the following parameters: $g_{xx} = g_{yy} = 2.060$, $g_{zz} = 2.025$, and $|D| = 0.018$ cm^{-1} (see the Supporting Information). Thus, **2** obtained by the deprotonation of **1** showed diradical character. We predict that **2** has two limiting resonance structures: the Ru^{III}–semiquinone–imido state, [Ru^{III}(NPh-bpa)(tBu$_2$sq)], and the Ru^{II}–semiquinone–anilino radical, [Ru^{II}(·NPh-bpa)(tBu$_2$sq)]. The diradical character detected by EPR spectroscopy must result from [Ru^{II}(·NPh-bpa)(tBu$_2$sq)], as [Ru^{III}(NPh-bpa)(tBu$_2$sq)] would be inactive toward EPR spectroscopy at 5 K owing to the strong antiferromagnetic interaction between Ru^{III} and the semiquinonate ligand.

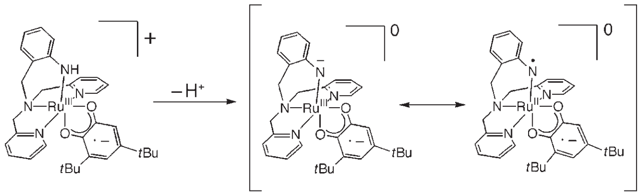

1 **2**

Scheme 2. Formation of **2** from **1** and limiting resonance structures of **2**.

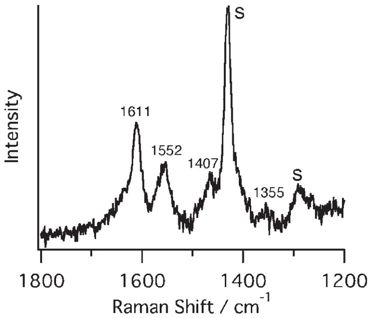

Figure 1. Resonance Raman spectrum of **2** in CH$_2$Cl$_2$ at 300 K with excitation at 514.5 nm. The solvent peaks are denoted with an "S".

The cyclic voltammogram of **2** in DME showed two quasireversible redox couples, at $E_{1/2} = -1.18$ and -0.37 V ($E_{1/2} = \frac{1}{2}(E_{pc}+E_{pc})$), which are assignable to the (Ru^{II}–cat)/(Ru^{II}–sq) and (Ru^{II}–sq)/(Ru^{III}–sq) redox couples, respectively, and an irreversible anodic wave at $E_{pa} = +0.72$ V (versus the saturated calomel electrode (SCE)). The cyclic voltammogram of the Ru^{III}–semiquinone–aniline complex **4** obtained by the treatment of **1** with CH$_3$SO$_3$H did not show an anodic wave at around +0.70 V. Thus, the irreversible wave observed for **2** at +0.72 V is correlated with the oxidation of the anilino-radical moiety.

The Ru^{II}–catechol–anilino radical complex [Ru^{II}(·NPh-bpa)(tBu$_2$cat)]$^-$ (**3**) was obtained by the electrochemical reduction of **2** in DME at −1.5 V (versus SCE). The UV/Vis/NIR spectrum of **3** in DME showed intense CT bands at 324 (11100), 432 (8470), 560 (7140), and 886 nm (6540 $\text{M}^{-1}\text{cm}^{-1}$). The ν_{8a} and ν_{7a} vibrational modes characteristic of an anilino radical were observed, as for **2**, in this case at 1605 and 1555 cm^{-1}, respectively. The EPR spectrum of **3** in DME at 20 K showed a rhombic pattern with $g_1 = 2.175$, $g_2 = 2.105$, and $g_3 = 1.950$ (Figure 2). The g_3 component is split into three signals as a result of hyperfine coupling with the N atom ($I = 1$) of the anilino-radical framework. A hyperfine-coupling constant, $A_{(N)}$, of 8.2 mT was measured.

Spin-density plots of **2** and **3** were obtained by DFT calculations (Figure 3). The two unpaired spins of **2** are spread mainly over the anilido moiety, the Ru center, and the dioxolene moiety. The amount of spin density on N, C2, C4, and C6 in the anilido moiety is 43, 8.0, 7.1, and 8.0%, respectively. The presence of unpaired-electron spin density in the dioxolene moiety of **2** and the absence of this spin density in the dioxolene moiety of **3** serve as good evidence for the semiquinone and catecolate binding modes in **2** and **3**, respectively. The main part of the unpaired spin of **3** was located at the anilido nitrogen atom and the ruthenium center; the amount of spin density on N and Ru was found to be 64 and 31%, respectively. The detection of a larger spin population at the anilido nitrogen atom than at the Ru center implies that **3** adopts the Ru^{II}–catechol–anilino radical state.

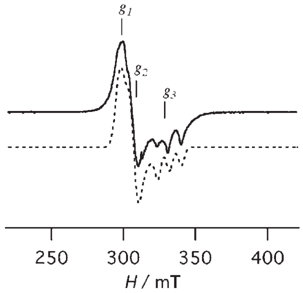

Figure 2. X-band EPR spectrum of **3** in DME at 20 K (solid line) and the simulation curve (dotted line) derived by using the parameters $g_1 = 2.175$, $g_2 = 2.105$, $g_3 = 1.950$, and $A_{(N)} = 8.2$ mT.

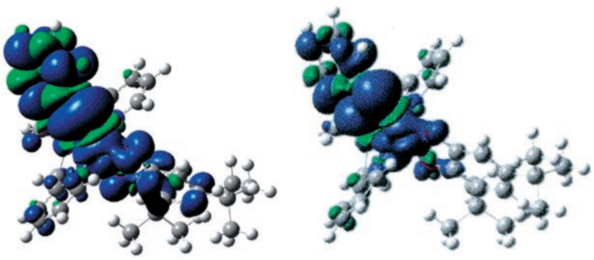

Figure 3. Spin-density plots of **2** (left) and **3** (right). The contour isovalue is 0.0004.

Experimental Section

Physical measurements: Elemental analysis was carried out at the Research Center for Molecular-Scale Nanoscience, Institute for Molecular Science. ESI-TOF mass spectra were obtained with a micromass LCT time-of-flight mass spectrometer. The X-ray photoelectron spectrum (XPS) was recorded with a VG Scientific Ltd ESCA LAB MK II instrument. $\mathrm{Mg}_{\mathrm{K}\alpha}$ radiation (1253.6 eV) at 14.5 kV and 20 mA was used as the X-ray excitation source. The magnetic measurements were carried out on a powder sample with a Quantum Design MPMS-7 magnetometer in the temperature range 2–300 K. A diamagnetic correction was applied by using the Pascal constants. The effective magnetic moment was calculated by using the equation $\mu_{\mathrm{eff}} = 2.828(\chi_M T)^{1/2}$. Electronic absorption spectra were recorded on a Shimadzu UV-3100PC spectrophotometer. Cyclic voltammograms were measured with an ALS/chi model 660 electrochemical analyzer. All measurements were made by using a three-electrode system in deaerated solvents containing tetra-*n*-butylammonium perchlorate (0.1 M) as a supporting electrolyte: a glassy-carbon electrode as the working electrode, a platinum wire as the counter electrode, and Ag/Ag^+ as the reference electrode. The reference electrode was calibrated with SCE, and the reported potentials were referenced against SCE. The EPR spectra were measured with a JEOL X-band spectrometer (JES-FA200) by using an attached variable-temperature apparatus. Resonance Raman spectra were obtained by excitation at 514.5 nm with an Ar laser (100 mW) and detected with a JASCO RTS-1000 laser Raman spectrophotometer equipped with a Princeton Instruments CCD detector cooled with liquid nitrogen.

$[\{\mathrm{Ru^{II}(NH_2Ph\text{-}bpa)}\}_2(\mu\text{-Cl})_2](\mathrm{PF_6})_2$: A solution of $\mathrm{NH_2Ph}$-bpa (0.1 g, 0.33 mmol) in EtOH (5 mL) was added to a suspension of $[\{(\mathrm{C_6H_6})\mathrm{RuCl_2}\}_2]$ (0.08 g, 0.16 mmol) in EtOH (30 mL), and the resulting mixture was stirred at 70 °C under N_2 for 6 h. $\mathrm{NH_4PF_6}$ (0.11 g, 0.66 mmol) was then added, and the reaction mixture was stirred at 50 °C under N_2 for 1 h. The resulting brown powder was filtered off and washed with EtOH and $\mathrm{Et_2O}$ to give the title complex (0.16 g), which was used for the preparation of **1** without purification. MS (ESI): *m*/*z* calcd for $[\{\mathrm{Ru^{II}(NH_2Ph\text{-}bpa)}\}_2\mathrm{Cl_2}]^{2+}$: 441.042; found: 441.110.

1: A mixture of $[\{\mathrm{Ru(NH_2Ph\text{-}bpa)}\}_2(\mu\text{-Cl})_2](\mathrm{PF_6})_2$ (0.4 g, 0.34 mmol) and $\mathrm{AgBF_4}$ (0.13 g, 0.68 mmol) in acetone (25 mL) was heated at reflux for 2 h. The precipitated AgCl was removed by filtration, 3,5-di-*tert*-butylcatecolate (0.15 g, 0.68 mmol) and *t*BuOLi (0.11 g, 1.36 mmol) were added to the filtrate, and the reaction mixture was stirred at room temperature under N_2 for 3 days. The resulting green solution was evaporated to dryness under reduced pressure, and the crude product was purified on a column of acidic alumina with $\mathrm{CH_2Cl_2}$/acetone as the eluent. The purple-colored fraction collected was evaporated to dryness, and the solid residue was dissolved in MeOH (10 mL). An aqueous solution of $\mathrm{NaClO_4}$ (20 mL, 0.1 M) was added to the solution, whereupon **1** (0.2 g, 27 %) precipitated as a purple powder. MS (ESI-TOF, $\mathrm{CH_2Cl_2}$): *m*/*z* calcd for $[\mathrm{Ru^{III}(NHPh\text{-}bpa)}(t\mathrm{Bu_2sq})]^+$: 625.213; found: 625.214; elemental analysis calcd (%) for $\mathrm{C_{33}H_{41}N_4ClO_7Ru}$: C 53.40, H 5.57, N 7.55; found: C 53.51, H 5.55, N 7.26.

2: A solution of **1** (45 mg, 0.04 mmol) in DME (5 mL) was added to a suspension of *t*BuOK (7 mg, 0.06 mmol) in DME (5 mL), and the reaction mixture was stirred at room temperature under N_2 for 6 h. The resulting greenish-brown solution was evaporated to dryness, and the residue was washed with diethyl ether. Recrystallization from acetone/hexane gave **2** (16 mg, 23 %) as a greenish-blue powder. elemental analysis calcd (%) for $\mathrm{C_{33}H_{43}N_4O_4Ru}$: C 59.98, H 6.56, N 8.48; found: C 60.33, H 6.21, N 8.04.

4: A solution of $\mathrm{CH_3SO_3H}$ (50 µL) in MeOH (1 mL) was added to **1** (0.2 g, 0.27 mmol) in MeOH (10 mL), and the resulting mixture was stirred at room temperature for 1 h. An aqueous solution of $\mathrm{NaClO_4}$ (0.1 M, 30 mL) was then added to the reaction mixture, whereupon **4** (0.12 g, 52 %) precipitated as blue microcrystals. MS (ESI-TOF, MeOH): *m*/*z* calcd for $[\mathrm{Ru^{III}(NH_2Ph\text{-}bpa)}(t\mathrm{Bu_2sq})]^{2+}$: 313.110; found: 313.098; elemental analysis calcd (%) for $\mathrm{C_{33}H_{44}N_4Cl_2O_{12}Ru}$: C 46.05, H 5.15, N 6.51; found: C 45.78, H 4.90, N 6.35.

DFT calculations of the structures and electronic properties of complexes **2** and **3** were carried out by using the Gaussian 03 suite of programs.[11] In particular, the hybrid UB3LYP method[12] was used together with the LANL2DZ basis set[13] and an ultrafine grid.

Received: April 12, 2007

Keywords: anilino radicals · dioxolene ligands · EPR spectroscopy · Raman spectroscopy · ruthenium

---

[1] *N-centered Radicals* (Ed.: Z. Alfassi), Wiley, New York, **1998**.

[2] a) T. Büttner, J. Geier, G. Frison, J. Harmer, C. Calle, A. Schweiger, H. Schönberg, H. Grützmacher, *Science* **2005**, *307*, 235–238; b) P. Maire, M. Königsmann, A. Sreekanth, J. Harmer, A. Schweiger, H. Grützmacher, *J. Am. Chem. Soc.* **2006**, *128*, 6578–6580; c) E. Kogut, H. L. Wiencko, L. Zhang, D. E. Cordeau, T. H. Warren, *J. Am. Chem. Soc.* **2005**, *127*, 235–238.

[3] F. N. Penkert, T. Weyhermüller, E. Bill, P. Hildebrandt, S. Lecomte, K. Wieghardt, *J. Am. Chem. Soc.* **2000**, *122*, 9663–9673.

[4] a) M. J. Ingleson, M. Pink, J. C. Huffman, H. Fan, K. G. Caulton, *Organometallics* **2006**, *25*, 1112–1119; b) W. Kaim, R. Gross, *Angew. Chem.* **1985**, *97*, 869–870; *Angew. Chem. Int. Ed. Engl.* **1985**, *24*, 856–858; c) R. Gross, W. Kaim, *Inorg. Chem.* **1987**, *26*, 3596.

[5] K. Kobayashi, H. Ohtsu, T. Wada, T. Kato, K. Tanaka, *J. Am. Chem. Soc.* **2003**, *125*, 6729–6739.

[6] T. Hino, T. Wada, T. Fujihara, K. Tanaka, *Chem. Lett.* **2004**, *33*, 1596–1597.

[7] Y. Miyazato, T. Wada, K. Tanaka, *Bull. Chem. Soc. Jpn.* **2006**, *79*, 745–747.

[8] S. C. Burdette, C. J. Frederickson, W. Bu, S. J. Lippard, *J. Am. Chem. Soc.* **2003**, *125*, 1778–1787.

[9] T. R. Weaver, T. J. Meyer, S. A. Adeyemi, G. M. Brown, R. P. Eckberg, W. E. Hatfield, E. C. Johnson, R. W. Murray, D. Untereker, *J. Am. Chem. Soc.* **1975**, *97*, 3039–3048.

[10] G. N. R. Tripathi, R. H. Schuler, *J. Chem. Phys.* **1987**, *86*, 3795–3800.

[11] Gaussian 03 (Revision D.0.1): M. J. Frisch et al., see the Supporting Information.

[12] A. D. Becke, *J. Chem. Phys.* **1993**, *98*, 5648; A. D. Becke, *Phys. Rev. A* **1988**, *38*, 3098; C. Lee, W. Yang, R. G. Parr, *Phys. Rev. B* **1988**, *37*, 785.

[13] P. J. Hay, W. R. Wadt, *J. Chem. Phys.* **1985**, *82*, 270; W. R. Wadt, P. J. Hay, *J. Chem. Phys.* **1985**, *82*, 284; P. J. Hay, W. R. Wadt, *J. Chem. Phys.* **1985**, *82*, 299; T. H. Dunning, Jr., P. J. Hay in *Modern Theoretical Chemistry*, *Vol. 3* (Ed.: H. F. Schaefer III), Plenum, New York, **1976**, pp. 1–28.